Chapter 4

Full tokamak discharge simulator

In this chapter, we present the combined full tokamak discharge simulator developed by combining DINA-CH and CRONOS. Although both codes have the same equilibrium and transport physics, they have been used in different research areas. DINA-CH is a non-linear free-boundary plasma equilibrium evolution code which self-consistently calculates dynamic response of the free-boundary equilibrium to currents flowing in the PF coil and surrounding conducting systems. CRONOS is an advanced transport modelling code which self-consistently calculates plasma profile evolution with source profiles. Theses two codes are combined maintaining their original strengths in each research area. Firstly, we introduce the plasma equilibrium and transport implemented in the both codes. Secondly, we present algorithms used for evolving the free-boundary plasma equilibrium in DINA-CH and the plasma transport in CRONOS. Lastly, we present the code coupling scheme and challenges met during the code integration. In this chapter, we derive 'standard' formulations of the plasma equilibrium and transport in MKS units. These formulations are compared with both CRONOS and DINA-CH ones which are additionally introduced in Appendix A. Units are omitted in deriving these formulations for simplicity.

4.1 Plasma equilibrium

Both DINA-CH and CRONOS calculate the plasma equilibrium using the non-linear Grad-Shafranov equation [1]. However, while CRONOS calculates 2D fixed boundary plasma equilibrium [64] taking the plasma boundary as an input, DINA-CH calculates 2D free-boundary

plasma equilibrium consistent with currents in the PF coil and surrounding conducting coil systems.

4.1.1 Non-linear Grad-Shafranov equation

The plasma equilibrium is determined by the following set of coupled equations assuming stationary ideal MHD conditions.

$$\mathbf{j} \times \mathbf{B} = \nabla p \tag{4.1}$$

$$\nabla \cdot \mathbf{B} = 0 \tag{4.2}$$

$$\nabla \times \mathbf{B} = \mu_0 \mathbf{j} \tag{4.3}$$

where p, $\mathbf{j}$ and $\mathbf{B}$ are respectively the plasma pressure, current density and magnetic field.

Introducing a flux function ψ defined as the poloidal flux per radian in ϕ and relating $\nabla \cdot \mathbf{B} = 0$ and $\mathbf{B} \cdot \nabla\psi = 0$, the poloidal component of the magnetic fields can be expressed as follows.

$$B_R = -\frac{1}{R}\frac{\partial \psi}{\partial z}, \; B_z = \frac{1}{R}\frac{\partial \psi}{\partial R}. \tag{4.4}$$

From the symmetry of $\mathbf{j}$ and $\mathbf{B}$ in the force balance equation, the poloidal component of the plasma current can be expressed using a current flux function f.

$$j_R = -\frac{1}{R}\frac{\partial f}{\partial z}, \; j_z = \frac{1}{R}\frac{\partial f}{\partial R}. \tag{4.5}$$

Comparing these relations with Ampère's law

$$j_R = -\frac{1}{\mu_0}\frac{\partial B_\phi}{\partial z}, \; j_z = \frac{1}{\mu_0 R}\frac{\partial (R B_\phi)}{\partial R}, \tag{4.6}$$

the current flux function f is given as

$$f = \frac{R B_\phi}{\mu_0}. \tag{4.7}$$

Since the plasma pressure p is a function of ψ, the poloidal current function f is also a function of ψ.

Decomposing the poloidal and toroidal components of the plasma current and magnetic fields in the force balance equation

$$\mathbf{j_p} \times \mathbf{i}_\phi B_\phi + j_\phi \mathbf{i}_\phi \times \mathbf{B_p} = \nabla p, \tag{4.8}$$

and substituting the poloidal components using the flux functions

$$\mathbf{B_p} = \frac{1}{R}(\nabla\psi \times \mathbf{i}_\phi) \text{ and } \mathbf{j_p} = \frac{1}{R}(\nabla f \times \mathbf{i}_\phi), \tag{4.9}$$

the force balance equation can be rewritten as

$$j_\phi = R\frac{dp}{d\psi} + \frac{\mu_0}{R} f \frac{df}{d\psi}. \tag{4.10}$$

The toroidal current density, j_ϕ, can also be written in terms of ψ using Ampère's law as follows

$$-\mu_0 R j_\phi = R\frac{\partial}{\partial R}\frac{1}{R}\frac{\psi}{\partial R} + \frac{\partial^2\psi}{\partial z^2}. \tag{4.11}$$

Substituting the j_ϕ into this equation, the non-linear Grad-Shafranov equation (standard formulation with MKS units) is written as

$$R\frac{\partial}{\partial R}\left(\frac{1}{R}\frac{\partial\psi}{\partial R}\right) + \frac{\partial^2\psi}{\partial z^2} = -\mu_0 R\left(R\frac{dp}{d\psi} - \frac{\mu_0}{2R}\frac{df^2}{d\psi}\right) = -\mu_0 R^2\frac{dp}{d\psi} - \mu_0^2 f\frac{df}{d\psi}. \tag{4.12}$$

The non-linear Grad-Shafranov equations in DINA-CH and CRONOS are derived using different units and expressions. The detail derivations are shown in Appendix A.1.

DINA-CH : CGS units

$$R\frac{\partial}{\partial R}\left(\frac{1}{R}\frac{\partial\psi}{\partial R}\right) + \frac{\partial^2\psi}{\partial z^2} = -4\pi R^2\frac{dp}{d\psi} - \frac{1}{2}\frac{dF^2}{d\psi} = -4\pi R^2\frac{dp}{d\psi} - \left(\frac{4\pi}{c}\right)^2 f\frac{df}{d\psi}, \tag{4.13}$$

where

$$F = RB_\phi = \frac{4\pi f}{c}.$$

CRONOS : MKS units

$$R\frac{\partial}{\partial R}\left(\frac{1}{R}\frac{\partial\psi}{\partial R}\right) + \frac{\partial^2\psi}{\partial z^2} = -R^2\frac{dp_1}{d\psi} - F\frac{dF}{d\psi} = -\mu_0 R^2\frac{dp}{d\psi} - \mu_0^2 f\frac{df}{d\psi}, \tag{4.14}$$

where

$$F = RB_\phi = \mu_0 f, \quad p_1 = \mu_0 p.$$

4.1.2 Free-boundary plasma equilibrium

The fixed boundary plasma equilibrium is determined by solving the non-linear Grad-Shafranov equation with the toroidal plasma current density j_ϕ for a given plasma boundary. In the case of calculating a free-boundary plasma equilibrium, external circuit currents are additionally taken into account in solving the Grad-Shafranov equation.

$$R\frac{\partial}{\partial R}\left(\frac{1}{R}\frac{\partial \psi}{\partial R}\right)+\frac{\partial^2 \psi}{\partial z^2}=\begin{cases}-\mu_0 R j_\phi & \text{if}(R,z)\in S\\ -\mu_0\sum_{i=1}^{N} R_i I_i \delta(R-R_i)\delta(z-z_i) & \text{if}(R,z)\notin S\end{cases} \tag{4.15}$$

where N external toroidal circuits with current I_i are located in the position (R_i, z_i). S is the poloidal cross-section of the plasma. The plasma boundary is iteratively determined by defining the boundary flux of the plasma.

4.2 Plasma transport

Both DINA-CH and CRONOS calculate the plasma transport by solving a set of coupled 1D plasma transport equations averaged on the magnetic flux surface, such as the plasma current diffusion, particle and heat transport. CRONOS is a transport modelling code, in which all the transport equations are self-consistently calculated while the evolution of the plasma boundary is given as an input. On the other hand, DINA-CH is a free-boundary plasma equilibrium evolution code which calculates the plasma current diffusion self-consistently with the evolution of the free-boundary plasma equilibrium. In this code, the coupling between the plasma current diffusion and the particle and heat transport is slightly relaxed to improve the computational performance.

4.2.1 Magnetic flux surface averaging technique

The average of an arbitrary quantity A over a magnetic surface S which is labeled by ρ is defined

$$\langle A\rangle=\frac{\partial}{\partial V}\int_V A dV=\frac{1}{V'}\int_S A\frac{dS}{|\nabla\rho|}, \tag{4.16}$$

where

$$V'=\frac{\partial V}{\partial \rho}=\int_S \frac{dS}{|\nabla\rho|}. \tag{4.17}$$

V is the volume enclosed inside the magnetic surface S. This averaging has the properties (see Appendix A.2 for proofs),

$$\langle \nabla \cdot \mathbf{H} \rangle = \frac{\partial}{\partial V} \langle \mathbf{H} \cdot \nabla V \rangle , \quad \forall \mathbf{H}, \tag{4.18}$$

$$\frac{d}{dt} \left(V' \langle A \rangle \right) = V' \left\langle \frac{\partial A}{\partial t} \right\rangle + \frac{\partial}{\partial \rho} \langle A \mathbf{u}_\rho \cdot \nabla V \rangle , \quad \forall A, \tag{4.19}$$

where d/dt is the time derivative at a fixed ρ and $\partial/\partial t$ is the time derivative at a fixed point (R, z). Using these properties, the 1D transport equations defined on the flux surface can have the time derivative d/dt.

The velocity of a constant ρ surface $\mathbf{u}_\rho$ is defined by

$$\frac{d\rho}{dt} = \frac{\partial \rho}{\partial t} + \mathbf{u}_\rho \cdot \nabla \rho = 0 \tag{4.20}$$

4.2.2 Magnetic field diffusion

The 1D magnetic field diffusion equation can be derived starting from the generalized Ohm's law averaged on the magnetic flux surface.

$$\langle \mathbf{j} \cdot \mathbf{B} \rangle = \sigma \langle \mathbf{E} \cdot \mathbf{B} \rangle + \langle \mathbf{j_{ni}} \cdot \mathbf{B} \rangle \tag{4.21}$$

Using the following definitions

$$\mathbf{B} = \mathbf{B_p} + \mathbf{B}_\phi = \frac{1}{R} \nabla \psi \times \mathbf{i}_\phi + B_\phi \mathbf{i}_\phi \tag{4.22}$$

$$\mathbf{j} = \mathbf{j_p} + \mathbf{j}_\phi = \frac{1}{R} \nabla f \times \mathbf{i}_\phi + j_\phi \mathbf{i}_\phi \tag{4.23}$$

$$\oint_C \mathbf{E} \cdot d\mathbf{l} = E_\phi \left(2\pi R \right) - 2\pi \frac{\partial \psi}{\partial t} = 0 \tag{4.24}$$

$$\frac{d\psi}{dt} = \frac{\partial \psi}{\partial t} + \mathbf{u}_\rho \cdot \nabla \psi \tag{4.25}$$

$$\frac{\partial \psi}{\partial t} + \mathbf{u}_\psi \cdot \nabla \psi = 0 \tag{4.26}$$

$$\nabla \psi = \nabla \rho \frac{\partial \psi}{\partial \rho} \tag{4.27}$$

$\langle \mathbf{j} \cdot \mathbf{B} \rangle$ is given as (see Appendix A.3)

$$\langle \mathbf{j} \cdot \mathbf{B} \rangle = -f^2 \frac{1}{V'} \frac{\partial}{\partial \rho} \left(\frac{c_2}{f} \frac{\partial \psi}{\partial \rho} \right), \tag{4.28}$$

where

$$c_2 = \left\langle \frac{|\nabla \rho|^2}{R^2} \right\rangle = \int_S \frac{|\nabla \rho|^2}{R^2} \frac{dS}{|\nabla \rho|}. \tag{4.29}$$

$\langle \mathbf{E} \cdot \mathbf{B} \rangle$ is given as (see Appendix A.3)

$$\langle \mathbf{E} \cdot \mathbf{B} \rangle = -\mu_0 f \left\langle \frac{1}{R^2} \right\rangle \frac{d\psi}{dt}. \tag{4.30}$$

Inserting these $\langle \mathbf{E} \cdot \mathbf{B} \rangle$ and $\langle \mathbf{j} \cdot \mathbf{B} \rangle$ into the generalized Ohm's law, we have

$$\begin{aligned} \frac{d\psi}{dt} &= -\frac{\langle \mathbf{j} \cdot \mathbf{B} \rangle}{\sigma \mu_0 f \left\langle \frac{1}{R^2} \right\rangle} + \frac{\langle \mathbf{j}_{\mathbf{ni}} \cdot \mathbf{B} \rangle}{\sigma \mu_0 f \left\langle \frac{1}{R^2} \right\rangle} \\ &= \frac{f}{\sigma \mu_0 \left\langle \frac{1}{R^2} \right\rangle V'} \frac{\partial}{\partial \rho} \left(\frac{c_2}{f} \frac{\partial \psi}{\partial \rho} \right) + \frac{\langle \mathbf{j}_{\mathbf{ni}} \cdot \mathbf{B} \rangle}{\sigma \mu_0 f \left\langle \frac{1}{R^2} \right\rangle} \\ &= \frac{f}{\sigma \mu_0 c_3} \frac{\partial}{\partial \rho} \left(\frac{c_2}{f} \frac{\partial \psi}{\partial \rho} \right) + \frac{V' \langle \mathbf{j}_{\mathbf{ni}} \cdot \mathbf{B} \rangle}{\sigma \mu_0 f c_3}, \end{aligned} \tag{4.31}$$

where

$$c_3 = \left\langle \frac{1}{R^2} \right\rangle V'. \tag{4.32}$$

The magnetic field diffusion equations in DINA-CH and CRONOS are respectively expressed as (see Appendix A.3)

DINA-CH : CGS units

$$\frac{d\psi}{dt} = \frac{c\, c_2 C_3}{4\pi\sigma} \frac{\partial^2 \psi}{\partial \rho^2} + \frac{c\, C_3^2 \rho}{4\pi\sigma} \frac{\partial}{\partial \rho} \left(\frac{c_2}{C_3 \rho} \right) \frac{\partial \psi}{\partial \rho} + \frac{V'}{4\pi\sigma\rho} \langle \mathbf{j}_{\mathbf{ni}} \cdot \mathbf{B} \rangle, \tag{4.33}$$

where $C_3 = c_3^{-1}$ and $f = c\rho/c_3$.

CRONOS : MKS units

$$\frac{d\psi}{dt} = \frac{c_2}{\sigma \mu_0 c_3} \frac{\partial^2 \psi}{\partial \rho^2} + \frac{F}{\sigma \mu_0 c_3} \frac{\partial}{\partial \rho} \left(\frac{c_2}{F} \right) \frac{\partial \psi}{\partial \rho} + \frac{V'}{\sigma F c_3} \langle \mathbf{j}_{\mathbf{ni}} \cdot \mathbf{B} \rangle, \tag{4.34}$$

where $F = RB_\phi = \mu_0 f$.

The evolution of the poloidal flux at the plasma boundary is given by

$$\begin{aligned}\frac{d\psi_b}{dt} &= \frac{d\psi_{pl}}{dt} + \frac{d\psi_{ext}}{dt} \\ &= \frac{d}{dt}\left(L_p I_p\right) + \frac{d\psi_{ext}}{dt}.\end{aligned} \tag{4.35}$$

Using an implicit discretization scheme

$$\frac{\psi_b^{n+1} - \psi_b^n}{\tau} = \frac{L_p^{n+1} I_p^{n+1} - L_p^n I_p^n}{\tau} + \frac{\psi_{ext}^{n+1} - \psi_{ext}^n}{\tau} \tag{4.36}$$

and the relation of the total plasma current (see appendix A.4)

$$I_p = -\frac{1}{2\pi\mu_0} c_2 V' \frac{\partial\psi}{\partial\rho}\bigg|_{\rho=\rho_b}, \tag{4.37}$$

the mixed boundary condition can be written as

$$\frac{1}{2\pi\mu_0} c_2 V' L_p^{n+1} \frac{\partial\psi}{\partial\rho}\bigg|_b^{n+1} + \psi_b^{n+1} = \psi_b^n + \psi_{ext}^{n+1} - \psi_{ext}^n - L_p^n I_p^n. \tag{4.38}$$

In the fixed boundary equilibrium case, there are usually 5 options for imposing the boundary condition:

1. Prescribe the external poloidal flux, ψ_{ext}^{n+1}.
2. Prescribe the boundary poloidal flux, $\psi_b(t)$.
3. Prescribe the boundary loop voltage, $V_{loop}(t) = -2\pi \frac{d\psi}{dt}\big|_b + \frac{1}{q_b}\frac{d\Phi}{dt}\big|_b$.
4. Prescribe the boundary surface voltage, $V_{surf}(t) = -2\pi \frac{d\psi}{dt}\big|_b$.
5. Prescribe the total plasma current, $I_p(t) = -\frac{1}{2\pi\mu_0} c_2 V' \frac{\partial\psi}{\partial\rho}\big|_b$.

In the free-boundary equilibrium case, the poloidal flux at the plasma boundary ψ_b^{n+1} is self-consistently calculated with the external poloidal flux ψ_{ext}^{n+1} provided by currents in the PF coil and surrounding conducting systems.

4.2.3 Particle transport

The evolution of the density of a species indicated by j is described by the continuity equation

$$\frac{\partial n_j}{\partial t} + \nabla \cdot (n_j \mathbf{u_j}) = S_j. \tag{4.39}$$

Averaging this equation over the flux surface and multiplying by V', we have

$$\left\langle \frac{\partial n_j}{\partial t} \right\rangle V' + \langle \nabla \cdot (n_j \mathbf{u_j}) \rangle V' = \langle S_j \rangle V'. \tag{4.40}$$

Using the properties of the flux surface average, this equation can be rewritten as

$$\frac{d}{dt}\left(V' \langle n_j \rangle\right) - \frac{\partial}{\partial \rho} \langle n_j \mathbf{u}_\rho \cdot \nabla V \rangle + \frac{\partial}{\partial V} \langle n_j \mathbf{u_j} \cdot \nabla V \rangle V' = \langle S_j \rangle V'. \tag{4.41}$$

Converting $\nabla V = \nabla \rho \dfrac{\partial V}{\partial \rho}$, this equation is further rewritten as

$$\frac{d}{dt}\left(V' \langle n_j \rangle\right) + \frac{\partial}{\partial \rho} \left[\langle n_j \left(\mathbf{u_j} - \mathbf{u}_\rho\right) \cdot \nabla \rho \rangle V'\right] = \langle S_j \rangle V'. \tag{4.42}$$

Defining the particle flux relative to a constant ρ surface by $\Gamma_j = \langle n_j \left(\mathbf{u_j} - \mathbf{u}_\rho\right) \cdot \nabla \rho \rangle$, the final equation can be simplified as

$$\frac{d}{dt}\left(n_j V'\right) + \frac{\partial}{\partial \rho}\left(\Gamma_j V'\right) = S_j V'. \tag{4.43}$$

Here the density and source are defined as functions of ρ. The particle flux can be defined as a sum of diffusion (D) and inward pinch velocity ($\mathbf{V_p}$) terms by

$$\mathbf{\Gamma_j} = n_j \left(\mathbf{u_j} - \mathbf{u}_\rho\right) = -D \nabla n_j + n_j \mathbf{V_p}. \tag{4.44}$$

Using this definition, the particle flux relative to a constant ρ surface is written as

$$\Gamma_j = -D \left\langle |\nabla \rho|^2 \right\rangle \frac{\partial n_j}{\partial \rho} + n_j \left\langle \mathbf{V_p} \cdot \nabla \rho \right\rangle. \tag{4.45}$$

The particle transport equations in DINA-CH and CRONOS are identical.

4.2.4 Electron heat transport

Neglecting the viscosity terms, the energy balance equation of the electrons can be written as

$$\frac{3}{2}\frac{\partial p_e}{\partial t} + \nabla \cdot \left(\mathbf{q_e} + \frac{5}{2} p_e \mathbf{u_e} \right) = \mathbf{j} \cdot \mathbf{E} - Q_{ei} - \mathbf{u_i} \cdot \nabla p_i + Q_e, \tag{4.46}$$

where p_e and p_i are respectively the electron and ion pressure. $\mathbf{u_e}$ and $\mathbf{u_i}$ are respectively the electron and ion velocities and $\mathbf{q_e}$ is the electron heat flux. Q_{ei} is the electron-ion equipartition power and Q_e is the electron heat source.

Since $\mathbf{j} = \mathbf{j_e} + \mathbf{j_i} \approx \mathbf{j_e}$, j^2 can be given as

DINA-CH : CGS units

$$j^2 = \mathbf{j} \cdot \mathbf{j} = \sigma_\parallel \left(\mathbf{E} + \frac{\mathbf{u_e} \times \mathbf{B}}{c} \right) \cdot \mathbf{j} = \sigma_\parallel \mathbf{E} \cdot \mathbf{j} + \sigma_\parallel \mathbf{u_e} \cdot \frac{(\mathbf{j} \times \mathbf{B})}{c} = \sigma_\parallel \mathbf{E} \cdot \mathbf{j} + \sigma_\parallel \mathbf{u_e} \cdot \nabla p \tag{4.47}$$

CRONOS : MKS units

$$j^2 = \mathbf{j} \cdot \mathbf{j} = \sigma_\parallel \left(\mathbf{E} + \mathbf{u_e} \times \mathbf{B} \right) \cdot \mathbf{j} = \sigma_\parallel \mathbf{E} \cdot \mathbf{j} + \sigma_\parallel \mathbf{u_e} \cdot (\mathbf{j} \times \mathbf{B}) = \sigma_\parallel \mathbf{E} \cdot \mathbf{j} + \sigma_\parallel \mathbf{u_e} \cdot \nabla p \tag{4.48}$$

From these equations, $\mathbf{j} \cdot \mathbf{E}$ is given as

$$\mathbf{j} \cdot \mathbf{E} = \mathbf{u_e} \cdot \nabla p + \frac{j^2}{\sigma_\parallel} = \mathbf{u_e} \cdot \nabla p + Q_{ohm}, \tag{4.49}$$

where Q_{ohm} is the ohmic heat source.

Using this expression, the energy balance equation of the electrons is rewritten as

$$\frac{3}{2}\frac{\partial p_e}{\partial t} + \nabla \cdot \left(\mathbf{q_e} + \frac{5}{2} p_e \mathbf{u_e} \right) - \mathbf{u_e} \cdot \nabla p + \mathbf{u_i} \cdot \nabla p_i = Q_e + Q_{ohm} - Q_{ei}. \tag{4.50}$$

Averaging this equation over the flux surface and multiplying by V', we have

$$\frac{3}{2}\left\langle \frac{\partial p_e}{\partial t} \right\rangle V' + \left\langle \nabla \cdot \left(\mathbf{q_e} + \frac{5}{2} p_e \mathbf{u_e} \right) \right\rangle V' - \left\langle \mathbf{u_e} \cdot \nabla p + \mathbf{u_i} \cdot \nabla p_i \right\rangle V' = \left\langle Q_e + Q_{ohm} - Q_{ei} \right\rangle V'. \tag{4.51}$$

The left-hand side of this equation can be rewritten as (see Appendix A.5)

$$\begin{aligned} &\frac{3}{2}\left\langle \frac{\partial p_e}{\partial t} \right\rangle V' + \left\langle \nabla \cdot \left(\mathbf{q_e} + \frac{5}{2} p_e \mathbf{u_e} \right) \right\rangle V' - \left\langle \mathbf{u_e} \cdot (\nabla p - \nabla p_i) \right\rangle V' \\ &= \frac{3}{2V'^{2/3}} \frac{d}{dt} \left(p_e V'^{5/3} \right) + \frac{\partial}{\partial \rho} \left[\left(q_e + \frac{5}{2} T_e \Gamma_e \right) V' \right] + \frac{\Gamma_e}{n_e} \frac{\partial p_e}{\partial \rho} V'. \end{aligned} \tag{4.52}$$

The electron heat transport equation is finally given by

$$\frac{3}{2}\frac{d}{dt}\left(p_e V'^{5/3}\right) + V'^{2/3}\frac{\partial}{\partial\rho}\left[\left(q_e + \frac{5}{2}T_e\Gamma_e\right)V'\right] = V'^{5/3}\left(Q_e + Q_{ohm} - Q_{ei} + \frac{\Gamma_e}{n_e}\frac{\partial p_e}{\partial\rho}\right). \quad (4.53)$$

In this equation, the electron heat flux and sources generally defined as

$$\mathbf{q_e} = -\chi_e n_e \nabla T_e - p_e V_e^q \nabla\rho, \quad (4.54)$$

$$q_e = \langle \mathbf{q_e}\cdot\nabla\rho\rangle = -\chi_e n_e \left\langle|\nabla\rho|^2\right\rangle \frac{\partial T_e}{\partial\rho} - p_e V_e^q \left\langle|\nabla\rho|^2\right\rangle, \quad (4.55)$$

$$Q_e = Q_{e,add} + Q_{e,fus} - Q_{line} - Q_{cyclo} - Q_{brem}, \quad (4.56)$$

where χ_e and V_e^q are respectively the electron heat conductivity and convective velocity. $Q_{e,add}$ and $Q_{e,fus}$ are respectively the additional electron heat source and alpha particle self-heating power to electrons. Q_{line}, Q_{cyclo} and Q_{brem} are respectively the line radiation, cyclotron and bremsstrahlung heat losses.

The electron heat transport equations in DINA-CH and CRONOS are identical.

4.2.5 Ion heat transport

Neglecting the viscosity terms, the energy balance equation of the ions can be written as

$$\frac{3}{2}\frac{\partial p_i}{\partial t} + \nabla\cdot\left(\mathbf{q_i} + \frac{5}{2}p_i\mathbf{u_i}\right) = Q_{ei} + \mathbf{u_i}\cdot\nabla p_i + Q_i, \quad (4.57)$$

where $\mathbf{q_i}$ is the ion heat flux and Q_i is the ion heat source. Averaging this equation over the flux surface and multiplying by V', we have

$$\frac{3}{2}\left\langle\frac{\partial p_i}{\partial t}\right\rangle V' + \left\langle\nabla\cdot\left(\mathbf{q_i} + \frac{5}{2}p_i\mathbf{u_i}\right)\right\rangle V' - \langle\mathbf{u_i}\cdot\nabla p_i\rangle V' = \langle Q_i + Q_{ei}\rangle V'. \quad (4.58)$$

The left hand side of the above equation is rewritten as (see Appendix A.6)

$$\begin{aligned}&\frac{3}{2}\left\langle\frac{\partial p_i}{\partial t}\right\rangle V' + \left\langle\nabla\cdot\left(\mathbf{q_i} + \frac{5}{2}p_i\mathbf{u_i}\right)\right\rangle V' - \langle\mathbf{u_i}\cdot\nabla p_i\rangle V' \\ &= \frac{3}{2V'^{2/3}}\frac{d}{dt}\left(p_i V'^{5/3}\right) + \frac{\partial}{\partial\rho}\left[\left(q_i + \frac{5}{2}T_i\Gamma_i\right)V'\right] + \frac{\Gamma_e}{n_e}\frac{\partial p_i}{\partial\rho}V'. \end{aligned} \quad (4.59)$$

The ion heat transport equation is finally given by

$$\frac{3}{2}\frac{d}{dt}\left(p_i V'^{5/3}\right) + V'^{2/3}\frac{\partial}{\partial\rho}\left[\left(q_i + \frac{5}{2}T_i\Gamma_i\right)V'\right] = V'^{5/3}\left(Q_i + Q_{ei} + \frac{\Gamma_e}{n_e}\frac{\partial p_i}{\partial\rho}\right). \quad (4.60)$$

In this equation, the ion heat flux and sources are generally given as

$$\mathbf{q_i} = -\chi_i n_i \nabla T_i - p_i V_i^q \nabla \rho, \tag{4.61}$$

$$q_e = \langle \mathbf{q_i} \cdot \nabla \rho \rangle = -\chi_i n_i \left\langle |\nabla \rho|^2 \right\rangle \frac{\partial T_i}{\partial \rho} - p_i V_i^q \left\langle |\nabla \rho|^2 \right\rangle, \tag{4.62}$$

$$Q_i = Q_{i,add} + Q_{i,fus}, \tag{4.63}$$

where χ_i and V_i^q are respectively the ion heat conductivity and convective velocity. $Q_{i,add}$ and $Q_{i,fus}$ are respectively the additional ion heat source and alpha particle self-heating power to ions.

The ion heat transport equations in DINA-CH and CRONOS are identical.

4.3 Plasma transport evolution scheme in CRONOS

The transport equations of the magnetic field, particles and heat can be rewritten in the following form which can be solved in either implicit or explicit mode.

$$\frac{dF}{dt} = A\frac{\partial^2 F}{\partial \rho^2} + B\frac{\partial F}{\partial \rho} + CF + D \tag{4.64}$$

The computational mode is defined by a scalar f in the range of $[0, 1]$.

$$f = \begin{cases} 0 & \text{Pure implicit} \\ 0.5 & \text{Crank-Nicolson} \\ 1 & \text{Pure explicit} \end{cases} \tag{4.65}$$

For the prediction of F_i^{n+1} located ith radial position at the time of $(n+1)\Delta t$, the above equation can be rewritten as

$$\frac{F_i^{n+1} - F_i^n}{\Delta t} = A_i^{n+f} \left.\frac{\partial^2 F}{\partial \rho^2}\right|_i^{n+f} + B_i^{n+f} \left.\frac{\partial F}{\partial \rho}\right|_i^{n+f} + C_i^{n+f} F_i^{n+f} + D_i^{n+f}. \tag{4.66}$$

Using the central difference scheme, the time derivatives are rewritten as

$$\left.\frac{\partial F}{\partial \rho}\right|_i^{n+f} = \frac{1}{2\Delta \rho}\left(F_{i+1}^{n+f} - F_{i-1}^{n+f}\right), \tag{4.67}$$

$$\left.\frac{\partial^2 F}{\partial \rho^2}\right|_i^{n+f} = \frac{1}{(\Delta\rho)^2}\left(F_{i+1}^{n+f} - 2F_i^{n+f} + F_{i-1}^{n+f}\right). \tag{4.68}$$

Using these relations, the differential equation can be simplified to the following form (see Appendix A.7)

$$a_i F_{i+1}^{n+1} + b_i F_i^{n+1} + c_i F_{i-1}^{n+1} = d_i. \tag{4.69}$$

The coefficients are given by

$$\begin{aligned}
a_i &= (1-f)\left(\frac{fA_i^n + (1-f)A_i^{n+1}}{(\Delta\rho)^2} + \frac{fB_i^n + (1-f)B_i^{n+1}}{2\Delta\rho}\right),\\
b_i &= (1-f)\left(-2\frac{fA_i^n + (1-f)A_i^{n+1}}{(\Delta\rho)^2} + fC_i^n + (1-f)C_i^{n+1}\right) - \frac{1}{\Delta t},\\
c_i &= (1-f)\left(\frac{fA_i^n + (1-f)A_i^{n+1}}{(\Delta\rho)^2} - \frac{fB_i^n + (1-f)B_i^{n+1}}{2\Delta\rho}\right),\\
d_i &= -f\left(\frac{fA_i^n + (1-f)A_i^{n+1}}{(\Delta\rho)^2} + \frac{fB_i^n + (1-f)B_i^{n+1}}{2\Delta\rho}\right)F_{i+1}^n\\
&\quad + \left\{-f\left(-2\frac{fA_i^n + (1-f)A_i^{n+1}}{(\Delta\rho)^2} + fC_i^n + (1-f)C_i^{n+1}\right) - \frac{1}{\Delta t}\right\}F_i^n\\
&\quad - f\left(\frac{fA_i^n + (1-f)A_i^{n+1}}{(\Delta\rho)^2} - \frac{fB_i^n + (1-f)B_i^{n+1}}{2\Delta\rho}\right)F_{i-1}^n\\
&\quad + fD_i^n + (1-f)D_i^{n+1}.
\end{aligned}$$

By collecting this relation for all radial points, a matrix relation can be constructed.

$$\begin{bmatrix}
b_0 & a_0 & 0 & \cdots & 0 & 0\\
c_1 & b_1 & a_1 & \cdots & 0 & 0\\
0 & c_2 & b_2 & \cdots & 0 & 0\\
\vdots & \vdots & \vdots & \ddots & \vdots & \vdots\\
0 & 0 & 0 & \cdots & b_{N-1} & a_{N-1}\\
0 & 0 & 0 & \cdots & c_N & b_N
\end{bmatrix}
\begin{bmatrix} F_0^{n+1}\\ F_1^{n+1}\\ F_2^{n+1}\\ \vdots\\ F_{N-1}^{n+1}\\ F_N^{n+1}\end{bmatrix}
=
\begin{bmatrix} d_0\\ d_1\\ d_2\\ \vdots\\ d_{N-1}\\ d_N\end{bmatrix}, \tag{4.70}$$

where the boundary condition is applied for $i = 1$ and N. The following scheme is used to solve this matrix relation with an implicit method:

1. Calculate the coefficients a_i, b_i ,c_i and d_i using the explicit method ($f = 1$) at the first iteration.

2. Calculate the explicit solution F_i^{n+1} by solving the matrix relation.

3. Recalculate the coefficients using the implicit method ($f \neq 1$) and F_i^{n+1}.
4. Calculate the implicit solution F_i^{n+1} by solving the matrix relation.
5. Repeat these procedures until a good convergence is achieved.
6. If the convergence is not achieved, decrease the transport time-step and restart from the first step.

4.4 Free-boundary plasma equilibrium evolution scheme in DINA-CH

To calculate the non-linear free-boundary plasma evolution, the free-boundary plasma equilibrium has to be self-consistently calculated with a set of the plasma transport equations and circuit equations for the PF coil and surrounding conducting systems. DINA-CH self-consistently calculates the magnetic field diffusion with the evolution of the free-boundary plasma equilibrium and circuit currents, using an iterative implicit scheme. The particle and heat transport are coupled to the free-boundary plasma equilibrium evolution using an explicit scheme.

4.4.1 Circuit equations

The toroidal current density in the ith axisymmetric external toroidal circuit located in the position (r_i, z_i) is given by

$$j_i = \sigma_i E_i, \tag{4.71}$$

where σ_i is the electrical conductivity. The toroidal electric field E_i is given by

$$E_i = \frac{1}{2\pi r_i}\left(-\frac{\partial \psi_i}{\partial t} + V_i\right), \tag{4.72}$$

where $-\partial\psi_i/\partial t$ is the induced voltage in the ith circuit and V_i is the applied voltage to the ith circuit. Using the definition of electrical resistivity of the element with the area S_i, $R_i = \sigma_i S_i / 2\pi r_i$, the above equation can be written as

$$-\frac{\partial \psi_i}{\partial t} + V_i = R_i I_i \tag{4.73}$$

The poloidal flux ψ_i for each current element is given by

$$\psi_i = L_i I_i + \sum_{j \neq i} M_{ij} I_j + \sum_k M_{ik}^{cp} I_k \tag{4.74}$$

where M_{ij} is the mutual inductance between the ith and jth conducting element, M_{ik}^{cp} is the mutual inductance between the ith conducting element and kth filament current in the plasma.

Combining the two equations and assuming the self-inductance and mutual inductance are time independent for a solid conductor, we can get the following equation.

$$L_i \frac{\partial I_i}{\partial t} + \sum_{j \neq i} M_{ij} \frac{\partial I_j}{\partial t} + \sum_k M_{ik}^{cp} \frac{\partial I_k}{\partial t} + R_i I_i = V_i \tag{4.75}$$

Using the matrix and vector notations, this equation is rewritten as

$$M \frac{\partial I_c}{\partial t} + M^{cp} \frac{\partial I_p}{\partial t} + R I_c = V_c \tag{4.76}$$

where

$$M = \begin{bmatrix} L_1 & M_{12} & \cdots & M_{1n_c} \\ M_{12} & L_2 & \cdots & M_{2n_c} \\ \vdots & \vdots & \ddots & \vdots \\ M_{1n_c} & M_{2n_c} & \cdots & L_{n_c} \end{bmatrix}, \quad M^{cp} = \begin{bmatrix} 0 & M_{12} & \cdots & M_{1n_p} \\ M_{12} & 0 & \cdots & M_{2n_p} \\ \vdots & \vdots & \ddots & \vdots \\ M_{n_c 1} & M_{n_c 2} & \cdots & 0 \end{bmatrix},$$

$$R = \begin{bmatrix} R_1 & 0 & \cdots & 0 \\ 0 & R_2 & \cdots & 0 \\ \vdots & \vdots & \ddots & \vdots \\ 0 & 0 & \cdots & R_{n_c} \end{bmatrix}, \quad I_c = \begin{bmatrix} I_1 \\ I_2 \\ \vdots \\ I_{n_c} \end{bmatrix}, \quad I_p = \begin{bmatrix} I_1 \\ I_2 \\ \vdots \\ I_{n_p} \end{bmatrix}, \text{ and } V_c = \begin{bmatrix} V_1 \\ V_2 \\ \vdots \\ V_{n_a} \\ 0 \\ \vdots \\ 0 \end{bmatrix}$$

The numbers of the conductors and plasma elements are respectively n_c and n_p. Voltages in the n_a active conductors can be non-zeros.

4.4.2 Free-boundary plasma equilibrium evolution algorithm

1. At the beginning of nth time-step, the following information is obtained from the previous $(n-1)$th time-step results: the toroidal current density $j_\phi(t_n, R, z) = j_{pl}(t_n, R, z) + j_{ext}(t_n, R, z)$, poloidal flux $\psi(t_n, R, z)$, normalized magnetic flux surface coordinate ($\rho(t_n, R, z)$, $\theta(t_n, R, z)$) and flux surface averaged 1D plasma profiles $\psi(t_n, \rho)$, $n_{e,i}(t_n, \rho)$ and $p_{e,i}(t_n, \rho)$.

2. At the beginning of sth iteration in the nth time-step, solve the magnetic field diffusion with a given time-step Δt to get the sth estimate of the poloidal flux for the $(n+1)$th time-step $\psi^{s*}(t_{n+1}, \rho)$.

   (a) For the first iteration ($s = 1$), use an explicit scheme with $\psi(t_n, \rho)$

   (b) From the second iteration ($s > 1$), use an implicit scheme with $\psi(t_n, \rho)$ and $\psi^{(s-1)}(t_{n+1}, \rho)$.

3. Calculate the plasma current $j_{pl}^{s*}(t_{n+1}, R, z)$ using the estimate of the poloidal flux.

4. Solve the circuit equations to get the external circuit current $j_{ext}^{s*}(t_{n+1}, R, z)$.

5. Solve the free-boundary G-S equation using $j_\phi^{s*}(t_{n+1}, R, z) = j_{pl}^{s*}(t_{n+1}, R, z) + j_{ext}^{s*}(t_{n+1}, R, z)$ to get the poloidal flux $\psi^s(t_{n+1}, R, z)$.

6. Calculate the normalized magnetic flux surface coordinate ($\rho^{s*}(t_{n+1}, R, z)$, $\theta^{s*}(t_{n+1}, R, z)$) and the flux surface averaged 1D plasma profiles, such as $\psi^{s*}(t_{n+1}, \rho)$, $n_{e,i}^{s*}(t_{n+1}, \rho)$ and $p_{e,i}^{s*}(t_{n+1}, \rho)$

7. Check the convergence condition for the poloidal flux given by

$$\left| \frac{\psi^s(t_{n+1}, R, z) - \psi^{(s-1)}(t_{n+1}, R, z)}{\psi^{(s-1)}(t_{n+1}, R, z)} \right| < \epsilon_\psi, \quad \forall (R, z). \tag{4.77}$$

   If the convergence condition is not satisfied, go to the step 2.

8. Calculate the particle and heat transport using an explicit scheme.

9. Check the constraint on the vertical plasma motion given by

$$\left| \frac{\dot{z}_{pl}(t_{n+1}) - \dot{z}_{pl}(t_n)}{\dot{z}_{pl}(t_n)} \right| < \epsilon_{\dot{z}_{pl}}, \tag{4.78}$$

where

$$z_{pl} = \frac{\int_S z j_{pl}(R,z) dS}{\int_S j_{pl}(R,z) dS}. \tag{4.79}$$

If this constraint is not satisfied, decrease the time-step Δt and go to the step 1. Otherwise, go to the next $(n+1)$th time-step.

4.5 Combined tokamak discharge simulator

Coupling two physics codes is a general method of studying the effect of non-linear coupling of the different physics represented by each code independently. However, this requires a reliable code coupling scheme to prevent the coupled system from being subjected to significant uncertainty caused by the coupling itself in conditions in which each code normally behaves correctly.

4.5.1 Code coupling scheme

In the combined tokamak discharge simulator, DINA-CH provides the non-linear evolution of the free-boundary plasma equilibrium self-consistently calculated with the plasma current diffusion, in response to both controlled PF coil currents and inductively driven currents in the surrounding conducting system. CRONOS provides the evolution of the plasma profiles by self-consistently solving heat and particle transport with source profiles. The free-boundary plasma equilibrium provided by DINA-CH is directly used for CRONOS transport and source calculations. The plasma and source profiles provided by CRONOS are directly used for DINA-CH in calculating the free-boundary equilibrium and current diffusion.

The code coupling scheme used for the combined tokamak discharge simulator is shown in figure 4.1. All the exchanged data between DINA-CH and CRONOS are passed as SIMULINK variables explicitly treated in time. Therefore, the heat and particle transport calculated by CRONOS and the plasma current diffusion are not implicitly coupled. This slightly deteriorates the consistency in implicitly solving a complete set of coupled transport equations. Nevertheless, this was an inevitable choice to guarantee computational performance and reliability of the combined tokamak discharge simulator. The computational performance of the combined simulation was not significantly deteriorated by the

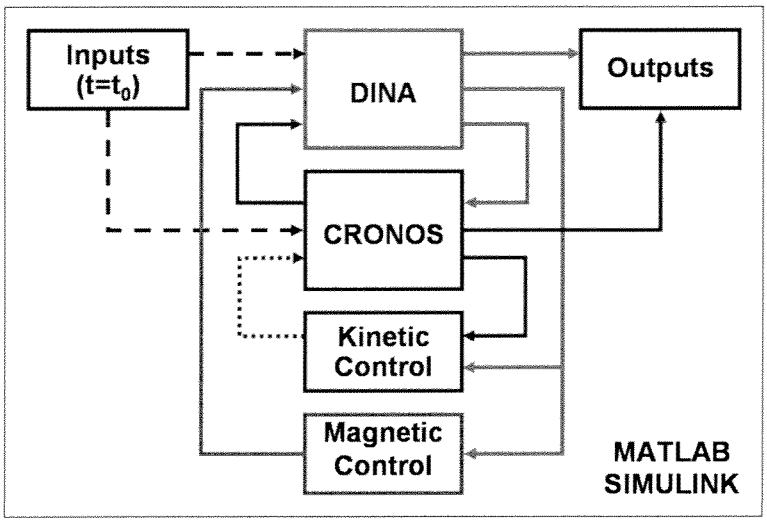

Figure 4.1: Code coupling scheme used for the combined tokamak discharge simulator. Inputs provide initial plasma equilibrium information only at the beginning of simulation (dashed lines). Control of the kinetic plasma profiles is not yet in the closed loop (dotted line).

explicit data exchange scheme and propagation of numerical errors between the two codes was avoided. With this code coupling scheme, the two codes were combined maintaining their original code structures.

Inputs for a full tokamak discharge simulation consist of initial plasma profiles and a reference operation scenario. The initial plasma profiles are prepared by performing a preliminary CRONOS simulation with a prescribed plasma boundary given by the reference operation scenario. The reference operation scenario provides guidance for the tokamak discharge evolution. The evolution of the total plasma current, position and shape are guided by pre-programmed PF coil current waveforms and also feedback controlled respecting their target waveforms. The average electron density evolution and the H&CD scheme are generally prescribed. At the first time-step, an initial free-boundary plasma equilibrium is calculated by DINA-CH with the input plasma profiles. In order to make the initial plasma boundary close to that given by the reference operation scenario, the initial currents in the PF coils are determined by trial. Initial eddy currents in the surrounding conducting systems are extrapolated back from the stationary currents built up after the simulation starts. Once the tokamak discharge simulation starts with a reasonable plasma configuration, the two codes exchange data at every subsequent time step.

This combined tokamak discharge simulator inherits much useful functionality from both

DINA-CH and CRONOS. DINA-CH provides magnetic diagnostic models, such as the magnetic probes and flux loops, and kinetic diagnostic models, such as the interferometer, bolometer and neutron camera. These measurements can be used for either magnetic or kinetic plasma control, by reconstructing the plasma equilibrium in the feedback loop. Magnetic plasma control provides PF coil voltages through the power supplies linked to the controllers for the total plasma current, position and shape. Kinetic plasma control, which is work in progress, provides auxiliary H&CD power for controlling the plasma profiles. Various auxiliary H&CD source modules, such as SINBAD [71, 72] for NBH&CD, PION [73] for ICRH&FWCD, DELPHINE [74] and LUKE [75] for LHH&CD, REMA [76] for ECH&CD and SPOT [77] for alpha particle self-heating, are available in CRONOS. CRONOS also provides various transport models based on either empirical formulation or theory, such as NCLASS [78], Weilend model [79], GLF23 [80] and KIAUTO [37]. Toroidal plasma rotation can be included into the set of coupled transport equations. The SIMULINK graphical user interface (see figure 4.2) of the combined DINA-CH and CRONOS simulator provides improved accessibility to this tokamak model for non-programmer users.

4.5.2 Challenges met during the code coupling

DINA-CH has a free-boundary equilibrium solver and CRONOS has a fixed boundary equilibrium solver. The same plasma equilibrium is implemented in the two codes with slightly different expressions and assumptions [23, 24, 25]. Therefore, in principle, CRONOS can reconstruct a DINA-CH free-boundary equilibrium taking the plasma boundary information and use it for its own plasma transport and source profile calculations. However, the reconstructed equilibrium would be slightly different from the original DINA-CH equilibrium and this inconsistency can be a possible seed for numerical errors in a time simulation. A safe coupling method avoiding this problem [65] is to directly provide the DINA-CH equilibrium for CRONOS transport and source calculations [66]. This also improves the computational performance and does not cause any loss of information in studying the physics as far as the selected code has superior functionality. The heat and particle transport solver in DINA-CH has to be turned off for the same reason.

The choice of data exchange scheme is another issue which has an influence on the computational performance, consistency and numerical stability. The simplest way to exchange data between two codes avoiding these difficulties is to use an explicit scheme in time. This

scheme does not require any additional iteration which can significantly deteriorate the computational performance and possibly cause continuous propagation of numerical errors. This is also useful for maintaining the original code structures and therefore to independently manage and upgrade each code. To ensure the convergence of this explicit data exchange scheme, a sufficiently small time-step is used.

Computational performance of the combined tokamak discharge simulations is reduced with respect to the sum of the independent computational performance of each code. DINA-CH already uses a fixed time-step in advancing the free-boundary plasma equilibrium evolution and has no modification which slowed down the computation, except preparing additional outputs for CRONOS. However, CRONOS, which originally used an advanced acceleration scheme while solving the plasma transport, is significantly slowed down by limiting the maximum time-step of the acceleration scheme. In the combined simulator, the fixed time-step of DINA-CH is used as the maximum time-step of the CRONOS acceleration scheme. In order to improve this computational performance, a time-varying source profile update interval is used. For a time-consuming source profile calculation, frequent source profile updating is only prescribed when the plasma state is changing fast or significantly enough. During the test of this idea, it was identified that several source profiles are erroneously dependent on the source profile update interval. This problem was resolved by upgrading the CRONOS source modules.

Several new numerical instabilities were observed in the combined tokamak discharge simulations. The SPIDER equilibrium solver [67] was adopted to resolve a numerical difficulty that occurred when treating a highly peaked edge bootstrap current profile in ITER. The density of the original 2D grid points used for calculating the free-boundary equilibrium was insufficient to correctly represent the peaked edge bootstrap current. As a new candidate to further improve the numerical stability, an adaptive grid solver is now being developed. Another numerical difficulty was identified in the heat transport calculation. This was an exceptional situation for a transport modelling code with a fixed boundary equilibrium solver, such as CRONOS. When a diverted plasma experiences a back-transition to a limited configuration and moves fast in the radial direction, the plasma temperature profile at the edge is set to a prescribed minimum value, resulting in a discontinuity in the radial gradient. The heat loss during a particular transport time-step was unexpectedly high. This difficulty was resolved by allowing the transport solver to use a much smaller internal time-step when the convergence is poor.

Validation of the combined tokamak discharge simulator for present experiments is a remaining issue. DINA-CH, originally used to study non-linear plasma responses to the plasma disturbances, was validated for TCV plasmas for the dynamic plasma response to PF coil voltage stimulation and non-linear evolution of the vertical displacement events (VDEs) [24, 34, 35, 36]. At the same time it was benchmarked against several linear plasma dynamic response models. The plasma transport modelling of CRONOS and its source calculation modules were validated for Tore Supra plasmas [25, 37, 38, 39] and benchmarked on JET experiments [68, 69, 70]. Although the combined tokamak discharge simulator has not yet been validated as a whole against present experiments, we have directly used it for simulating ITER discharges. The code coupling scheme used for this simulator does not appear to add any significant additional uncertainty which invalidates the previously conducted validation of each code, since each code in the combined simulator still keeps its original structure and physics by treating the exchanged data explicitly in time. The exchanged data in the combined simulation simply plays a role of experimental inputs in an independently conducted simulation using the original code. We will demonstrated the capability of the combined tokamak discharge simulator by simulating ITER scenario 2 in chapter 5, as well as the 12MA hybrid mode scenario in chapter 7 of this thesis.

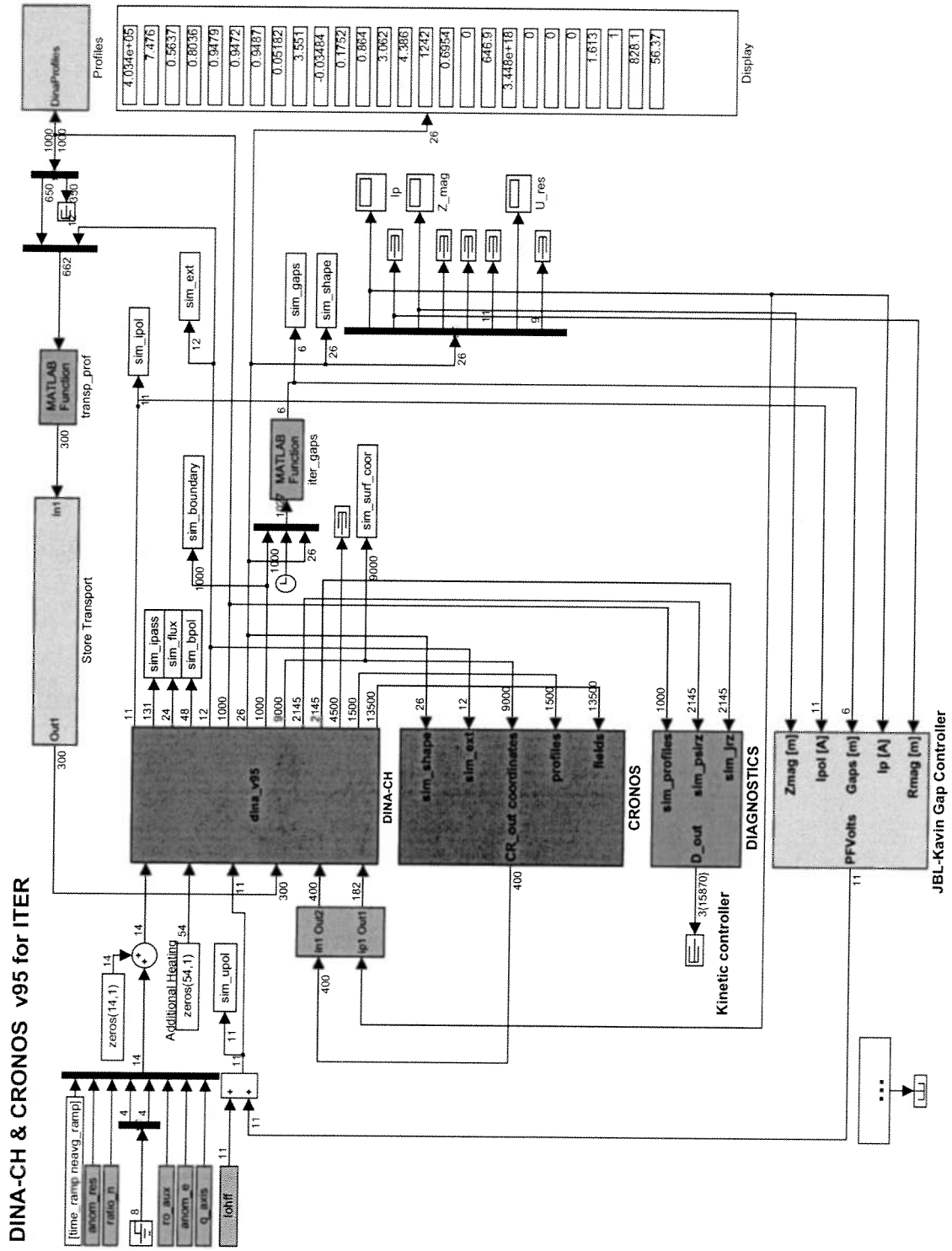

Figure 4.2: Simulink model of ITER in the combined tokamak discharge simulator